Amphibole Control on Copper Systematics in Arcs: Insights from the Analysis of Global Datasets

Nicholas D. Barber[1*], Marie Edmonds[1], Frances Jenner[2], Andreas Audétat[3], and Helen Williams[1]

[1]Department of Earth Sciences, University of Cambridge

[2]School of Environment, Earth, and Ecosystem Sciences, The Open University

[3]Bayerisches Geoinstitut, University of Bayreuth

January 5th, 2021

This manuscript has been submitted for publication in Geochimica et Cosmochimica Acta as of January 5th, 2021. Please note that this manuscript is still under review. An earlier version of the manuscript was rejected with constructive comments from Nature Communications. Subsequent versions of this manuscript may have slightly different content than the original version. If accepted, the final version of this manuscript will be available via the 'Peer-reviewed Publication DOI' link on the right-hand side of this webpage. Please feel free to contact Nick (ndb38@cam.ac.uk) with any feedback. We welcome your comments!

Abstract

Copper, sourced from porphyry deposits formed in arc settings, is a critical resource. The processes that shape the copper contents of magmas remain poorly understood. Existing models place emphasis on different petrological agents that explain large-scale trends in copper systematics. Previous studies have noted the 'Cu paradox,' where the magmas with high Sr/Y ratios, indicative of ore-forming potential, have the lowest copper concentrations. Here we compile a multidimensional database of volcanic whole rock compositions and couple it with simple petrological models to elucidate the controls on volcanic whole rock compositions with respect to Cu. We show that calc-alkaline, high Sr/Y magmas undergo iron depletion caused by extensive amphibole and/or garnet fractionation, which promotes sulphide fractionation and copper depletion. We demonstrate the importance of amphibole fractionation as a globally important process that promotes both calc-alkaline differentiation and sulphide fractionation in arc magmas; and its role in pre-conditioning magmas that ultimately feed copper porphyry deposits. Despite their paucity in copper, high Sr/Y magmas are associated with porphyry deposits, implying that the propensity of magmas to form such deposits depends on factors other than a magma's bulk copper content.

1 Introduction

Copper (Cu) is economically important owing to its role in the development of electrical components and its critical status in the transition to green energy[1]. Porphyry deposits, which are temporally and spatially associated with arc magmatism (Figure 1), account for over 70% of global Cu ore production[2], and significant amounts of Au and Mo[2]. A general unifying theory to describe the formation of porphyry deposits in arcs is lacking[3]. Prevailing magmatic models of Cu porphyry formation focus on two important processes, which may promote Cu enrichment, transport, and deposition in and around porphyry stocks porphyry stocks: (i) the saturation of the magma in sulphide (an Fe and S-bearing liquid or mineral phase), into which Cu partitions strongly[4–10], a process which may deplete the magma Cu when sulphide fractionates, but may also enrich a magma if sulphide is remobilised in hotter, or more oxidised magma[11–14]; and (ii) the exsolution of a volatile phase, which may unmix to a brine and vapor at low pressure[3], into which Cu and other metals partition and eventually precipitate from, leading to ore deposition[15–18].

A number of models have been proposed to explain how these processes may enhance a magma's ore potential. It has recently been suggested that sulphide saturation may be avoided by simultaneous Fe depletion and auto-oxidation caused by garnet fractionation[19]. Garnet's preference for Fe^{2+} leaves residual magmas enriched in Fe^{3+}[19]. This in turn produces a more oxidized, evolved melt (with higher S^{6+}/S^{2-}), which pushes the magma further away from sulphide saturation and may even trigger the dissolution of existing sulphides. It was proposed that this garnet-mediated process could enrich the melt in Cu, which could then be transferred to fluids when porphyry formation commences[19]. Alternatively, others have argued that sulphide accumulation may be critical to later ore development by pre-concentrating a reservoir of localized sulphides at

the base of a magma reservoir[11], where it is remobilised by intruding hotter or more oxidised magmas, thereby enriching the magma in Cu[11]. However, other studies have de-emphasized the importance of magmatic Cu contents as an indicator of ore potential[20,21], promoting instead the importance of magmatic water content[22–24], time scales of magma differentiation[25], and larger magma volumes[26]. Nonetheless, nearly all models agree that the process of sulphide saturation is important for understanding eventual ore formation. Sulphide saturation is a complex process mediated by temperature, pressure, and silicate melt composition, but which is increasingly well characterized by experiments and modeling[27–29]. However, it is presently unclear (i) what petrological processes in arc magmas will promote or delay sulphide fractionation, and (ii) whether the fractionation of a sulphide, and associated loss of Cu, is detrimental to later porphyry formation.

One reason that these outstanding questions remain is the measure of sample bias in our existing understanding of Cu systematics. Crucially, we need to establish what generic petrological processes, if any, can explain the abundances of Cu in ore fertile magmas in all major subduction zones, not just those in thick crust, for example. In order to address this need, we compiled a large global database of volcanic arc whole rock compositions (Figure 1). The ArcMetals database (N = 55,795) contains data from 17 arcs, encompassing geochemical and contextual information such as major, trace element and radiogenic isotope compositions, geology, location, and geologic age (see Methods), expanding on the approach taken by[14,19,20,30]. Combined, these parameters allow us to explore Cu systematics in all arc settings. We interpret the generic features of our global dataset with respect to Cu systematics using models of sulphide saturation based on experimental arc liquid lines of descent. This work pushes forward our understanding of key arc processes that influence magma fertility; and provides a

framework for further interrogation of chalcophile behaviour in specific volcanic arcs.

2 Methods

2.1 ArcMetals: Data Sources and Compilation

2.1.1 Database Design

This paper presents a new compilation of existing arc volcanic whole rock chemistry called *ArcMetals*. Our database was compiled with several crucial design distinctions in mind which distinguishes it from previous databases. First, we wanted the database to be fully integrated with the spatial dimension of the data. Hence, much of our compilation work takes place in a Geographic Information System (GIS) environment, where we can control and append geophysical and tectonic datasets. As discussed in greater detail both below and in the Supplement, this approach afford us several advantages over prior compilations. Here we take advantage of recent advances in the application of data science and Geographic Information Systems (GIS) in geochemistry, allowing us to build on prior studies that were based on simpler data compilation routines[14,19,20,23,30,31]. in the initial compilation and filtration of GeoRoc data, combining existing petrological datasets in ore systematic ways. Subsequently, we apply a range of geospatial techniques to append the maximum amount of geophysical data to our compilation without compromising the extent or quality of our data. This latter step is documented in detail in the Supplement, and is what sets this compilation apart from many previous datasets.

2.1.2 Geochemistry

Sample geochemical and analytical data were collected from the GeoRoc ([32]) database. These data were compiled using open source python code, available on GitHub (see link). Initially, 19 arc magma datasets were included in the database, but the Kermadec and Banda files contained so few data upon filtering, that they were ultimately omitted (Figure 1). Data for arc volcanic were compiled (see Supporting Info). Before filtering, the fully compiled database contained $>$ 200,000 records. In order to maximize the number of measurements per sample, we applied six filters to the initial compilation: (1) records with data obtained before 1960 C.E. were removed; (2) records with no recorded analytical technique were removed; (3) only those records pertaining to measurements by X-ray fluorescence (XRF), secondary ion mass spectrometry (SIMS), electron microprobe (EPMA), thermal ionization mass spectrometry (TIMS), inductively-coupled plasma mass spectrometry (ICP MS), laser ablation inductively-coupled plasma mass spectrometry (LA ICP MS), and Fourier transform infra red (FTIR) spectroscopy were retained; (4) the database was reduced to individual records where sample name, material type (whole rock, glass, or inclusion), and analytical technique were the same (e.g. if 1 whole rock sample had 4 records in GeoRoc measured using XRF, this filter would reduce the 4 records to one average for XRF); (5) records with the same sample name and material type were averaged and collapsed into one record. This had the effect of combining a sample's ICPMS measured trace elements with its XRF derived major elements; (6) samples that had the same element measured more than once using the same technique were removed. This filter only affected a small subset (a few hundred) samples, but having it in place makes it easier to quantify analytical errors (see SI). See the Supplemental Information section for more details. Before plotting the final database was filtered to only include those

magma's with a reported loss on ignition (LOI) less than 3.5 wt.%, following standards in the literature[23]

2.1.3 Geophysical Parameters

Several global geophysical datasets were appended to the main database using the geospatial software Quantum Geographic Information System, or QGIS 3.10. The data appended included subducting slab surfaces & geometry generated from extensive seismic records (slab dip, depth to slab, slab thickness)[33] , crustal thickness ([34]), and subducting plate sediment cover thickness ([35]). Every sample record in the database was linked to the geophysical datasets, which have good global coverage at a resolution of 10-100 km^2. A sub-population of database records had additional geophysical data appended based on their proximity to volcanoes analyzed in Syracuse et al. 2006[36]. These data included convergence rate, slab thermal parameter, and slab age[36]. The full QGIS methods and compilation scripts can be found in the Supplementary Information Section.

3 Results

We show our compilations of global volcanic whole rock geochemical data in Figures 2-5. These are discussed and interpreted in section 4. Figure 2a shows volcanic whole rock Sr/Y versus SiO_2, colour-coded for the different arcs (Figure 2b), Cu content (Figure 2c) and crustal thickness (Figure 2d). It has been shown that Cu-fertile magmas (magmas that are capable of forming porphyry-Cu deposits) have high whole rock Sr/Y ratios at intermediate to felsic magma compositions (Figure 2,[23,30,37]). The Sr/Y ratio, which compares the Large Ion Lithophile Element (LILE) Sr to the high field strength element (HFSE) Y, is widely regarded as a proxy for high pressure fractionation of hydrous arc magmas[14,23,37]. Strontium abundances during fractionation are controlled by

plagioclase[38], whereas Y abundances are controlled primarily by amphibole and garnet, as well as some minor phases like titanite[39]. The ratio of plagioclase to amphibole crystallized in a fractionating arc magma is depressed under conditions of high H_2O activity[40,41], and simultaneously stabilizes amphibole phases which incorporate H_2O into their structure[42]. Thus, a hydrous magma should see abundant amphibole fractionation early in its differentiation in the mid to deep crust (up to 50 km.,[43,44]) and late-stage plagioclase crystallization at or near volatile saturation in the upper crust[23]. This fractionation sequence will result in an elevated Sr/Y ratio in deeply derived, andesitic to dacitic magmas[23].

In Figure 3 we show MgO versus total FeO plots for global volcanic arc whole rocks, colour-coded for Cu contents (Figure 3a and c), Sr/Y (Figure 3b) and crustal thickness (CT; Figure 3d). These plots show that whole rocks with high Cu contents lie along a tholeiitic trend (with Fe-enrichment), whereas those whole rocks that lie along the calc-alkaline trajectory (with Fe depletion) are copper-poor; these rocks have highest Sr/Y, indicating the highest ore potential[23]. These findings are consistent with previous work[14,19,20,45,46].

We can identify the principal processes responsible for the geochemical trends shown in Figures 2 and 3 using rare earth element (REE) concentrations (Figures 4 and 5). The schemes at the top of both Figures 4 and 5 show vectors for the fractionation of garnet, amphibole, olivine, plagioclase, orthopyroxene and clinopyroxene using an index of REE plot curvature called Dy/Dy*[47]. Essentially, Dy/Dy* estimates the relative depletion of the middle rare earth (MREE) Dy in relation to its light and heavy counterparts (see the Methods section for details). The measure makes a weighted determination of the slope and shape of an REE spider plot with respect to Dy, as:

$$\frac{Dy}{Dy*} = \frac{Dy_N}{La_N^{4/13} + Yb_N^{9/13}}$$

.

Dy/Dy* is of particular use for tracking amphibole and garnet fractionation[19,47–49] (See Figure 4). Additionally, we plot the trajectories for melting in the garnet source field following[47]. The ratio Dy/Dy* tends to be lowered by amphibole and clinopyroxene fractionation. These same phases will deplete Dy relative to Yb. Olivine, plagioclase, and orthopyroxene will drive Dy/Dy* towards higher values, as these phases do not incorporate Dy into their structure and thus Dy will be enhanced relative to light (LREE) and heavy (HREE) rare earth elements. Garnet fractionation will move Dy/Yb to higher values during fractionation (i.e. deplete Yb relative to Dy) while simultaneously increasing Dy/Dy*. Mantle melting in the presence of garnet will lead to more moderate values if a garnet rich source is extensively melted.

The REE systematics of the global database can be further explored using a statistical approach[50], which compares parameters describing the shape of chrondrite-normalized multi-REE plots (Figure 5). The REE polynomials, symbolized by λ, describe the shape of REE curves[50] based on multivariate statistics across all REE elements[50] The polynomials are determined from the following calculation in orthogonal form:

$$\ln([\mathrm{REE}]/[\mathrm{REE}]_{\mathrm{CI}}) = \lambda_0 + \lambda_1 \mathrm{f}_1^{\mathrm{orth}} + \lambda_2 \mathrm{f}_2^{\mathrm{orth}} + \ldots$$

Where the f variables represents polynomials of REE atomic radius (r_{REE}), chosen to avoid co-correlation of the λs[50]. A schematic at the top of Figure 5 shows the effect of fractionation of amphibole and garnet on REE systematics, expressed in terms of $\lambda 1$ and $\lambda 2$. Figure 5 is subsampled to only color magmas for Cu (Figure 5a) and Sr/Y (Figure 5b) where the whole rock composition show Sr/Y > 50. In the section below we discuss these geochemical data, present an interpretative framework, and show how our work may be placed within the

context of previous studies.

4 Discussion

4.1 Geochemical Characteristics of High Sr/Y Magmas

We follow the lead of Loucks et al (2014), in recognizing the close association between high Sr/Y magmas and porphyry mineralization (Figure 2a[23]). Following their approach, we show that in our global database, high Sr/Y magmas show an association with continental arcs such as Mexico, the Andes and the Cascades (Figure 2b and Supplementary Material), a low mean whole rock Cu concentration ($<$ 50 ppm) (Figure 2c), and thicker crust (mean 40 km, Figure 2d), consistent with previous studies[14,20,30].

The mean Cu concentrations in Figure 2 were compared using a two-way analysis of variance (ANOVA) hypothesis test, and subsequent Tukey's highly significant difference test. The null hypothesis tested in all cases was that the mean of a given measure is the same between two groups. The likelihood this is due to random chance is calculated using an F statistic, given by:

$$F = \frac{\Sigma n_j \left(\bar{X}_j - \bar{X}\right)^2 / (k-1)}{\sum \Sigma \left(X - \bar{X}_j\right)^2 / (N-k)}$$

,

Where n_j = the sample size in the j^{th} group, $\bar{X}_j$ is the sample mean in the j^{th} group, $\bar{X}$ is the overall mean, k is the number of independent groups in the analysis, and N is the total number of observations in the analysis[51]. This F-statistic is compared to a a critical-F at a given confidence threshold and degrees of freedom. After determining the p-value, which is a simple but easily misinterpreted measure of the likelihood a difference between the means occurring due to random chance, the difference between the different treatments

(e.g. different arcs) is compared using a Tukey HSD test, which calculates the following test statistic:

$$q_s = \frac{Y_A - Y_B}{SE}$$

,

where Y_A is the larger of the two means, Y_B the smaller, and SE the standard error of the sum of the means. See the Supporting Information for detailed plots comparing the test statistics, tables with statistical outputs and constraints, and the code used in these analyses. The mean Cu and crustal thickness of the high and low ore fertility groups in Figures 2c and 2d have been compared, respectively, using ANOVA tests, and have all been shown to be statistically significant ($p \ll 0.005$) (see Supplementary Information for statistical tables).

The low mean Cu concentrations ([Cu]) in whole rocks associated with higher Sr/Y (Figure 2c) highlights the so-called 'Cu-paradox'[19] where Cu is present in low abundance in the magmas that appear to be most capable of forming ore deposits. Observations such as these have been used to support porphyry formation models where crystallization of sulphide removes Cu from the silicate melts, to be later remobilized by one of several petrological processes[11–13,19]. However, it is also possible that melt [Cu] depletion may have little bearing on whether a magma goes on to form an ore deposit[20,21]. While this initial analysis confirms the findings of prior studies that magmatic [Cu] is significantly lower in high Sr/Y magmas on a global scale[19,20], the petrological processes driving this association have not yet been resolved. Below, we apply our global dataset and a simple trace element partitioning model to better understand what processes are associated with high Sr/Y and inferred ore fertility.

Globally, it can be seen that both low Cu (Figure 3a) and high Sr/Y (Figure 3b) volcanic whole rocks follow a calc-alkaline path, showing consistent Fe loss

with decreasing [MgO] (paralleling the high Sr/Y ellipse in Figure 3d). Similar results were obtained by earlier data compilations[14,19,24,30]. In Figure 3c and 3d we plot the binned FeO and MgO concentrations that have been smoothed to show average FeO, MgO, Cu (Figure 3c), and crustal thickness (Figure 3d) at 0.05 wt.% MgO intervals. Figure 3c also shows that the fractional crystallization paths of experimentally synthesized and oxidized andesites and basalts[52], which also lie on the calc-alkaline trend displayed by high potential (high Sr/Y) magmas (more detail in section 4.3.1).

4.2 Amphibole vs. Garnet Signatures

Our global dataset suggests that high Sr/Y arc magmas share key petrological features: they may be produced from garnet-rich mantle source regions (plotting in the lower right quadrant of figure 4); undergo extensive fractionation of amphibole +/- garnet (they extend into the bottom left quadrant for Figure 4, upper right in Figure 5); and develop low Cu abundances during progressive fractional crystallisation (Figure 4a, 5a). While there is a clear association between high Sr/Y, low Cu magmas and the amphibole fractionation field, the location of high Sr/Y magmas at low Dy/Dy* and moderate Dy/Yb can also be explained through a magma formed in the "melting of mantle garnet" field (bottom right quadrant) which subsequently experienced (1) garnet fractionation at pressures $>$ 1.2 GPa[53], followed by (2) amphibole fractionation at lower pressures[53]. This sequence may only be piecemeal at shallower pressures, where amphibole will dominate as a fractionating phase, because garnet will not be stable[53]. Thus, while we will shortly demonstrate the importance of amphibole in these systems, garnet likely also plays an important role, especially under higher pressures[19,54].

Whole rock compositions with the highest Sr/Y ratios are characterized by

concave-up REE profiles, where there is both HREE depletion and overall enrichment in the LREE (Figure 4). Figure 4 shows a strong preference for high Sr/Y magmas to sit in the bottom right quadrant (High Dy/Yb, low Dy/Dy*), and Figure 5a and 5b show many high Sr/Y whole rocks sitting near the amphibole fractionation and garnet source field in $\lambda 1$ vs. $\lambda 2$ space (higher $\lambda 1$, higher $\lambda 2$). It is important to keep in mind that clinopyroxene will drive many of these REE trends in the same direction, whether in Dy/Dy* or λ space. However, clinopyroxene is less stable at lower temperatures[52,53], and amphibole is increasingly stabilized with greater water concentrations[52,53].

Garnet fractionation has gained popularity in the recent literature as a potential ore fertility mechanism[19,48,54]. Experiments have shown that garnet is stabilized as a fractionating phase at pressures above 1.2 GPa (approximately 42 km. depth)[53,55] and where melt water contents are high (above 4 wt. %)[53]. Direct evidence of garnet in arc magmas is rarely found in modern volcanics, but it has been found commonly in fossil arc systems[56]. Whether ancient or modern, where garnet can be seen widely in arc systems is in the lower crust cumulate lithologies of exhumed "arc roots," sections like the type section in Kohistan, Pakistan[57]. Models developed for the mantle wedge underlying Central America found evidence for the presence of mantle heterogeneities rich in garnet-peridotite or garnet pyroxenite lithologies[58]. Such mantle garnet "veins" would impart a garnet fingerprint on the resultant magmatic REE abundances if tapped by melting[58].

While we do not dispute the role of garnet fractionation to explain the occurrence of some magmas with low [Cu] in thicker-crust arcs[19,54], we suggest that amphibole is also an important candidate for moderating global arc Cu systematics as shown in Figures 4 and 5. This is not a new idea, having been proposed in the context of porphyry deposits[23] and the broader controls on mag-

matic Fe[20], though in both of those cases REEs were not used as a metric to measure amphibole's presence. Amphibole fractionates in many arc magmatic environments at moderate (15-40) depths[43,53], while also being verifiable petrographically in volcanic products. For many of the reasons the garnet hypothesis is favored, amphibole can be similarly supported as an important chemical control on the bulk chemistry of arc magmas. Amphibole will be stabilised at high temperature (between 900 and 1100 °C[52,53]), moderate to high pressure (0.7 - 1 GPa[43,53]), and high water contents[53]. Additionally, experimental work has already implicated amphibole as the dominant phase controlling major element characteristics in high pressure calc-alkaline magmas[53]. Our preference for amphibole does not preclude the importance of garnet or clinopyroxene fractionation, but clearly show the strong and unambiguous importance of the association between amphibole and high Sr/Y magmas, as has been argued in[14,20,22,23]. However, the mechanism by which amphibole obtains such an association has been overlooked in previous studies.

4.3 Amphibole Control on Sulphide Stability

4.3.1 Empirically Constrained Model

To understand how amphibole is able to affect these global Cu trends, it is necessary to show how amphibole can provide a mechanistic link between high Sr/Y, calc-alkaline, potentially ore forming magmas, and their low Cu contents. We do this using the empirical data from Ulmer et al. 2018[52] as the "starting ingredients" in a simple trace element partitioning model, which tracks to Cu, Ni, Sr, Y, and REE concentrations in three experimental assemblages. We then take the outputs of this trace element model, and feed them into a sulphide stability equation to calculate how stable theoretical sulphides are under these amphibole-fractionating conditions. Our goal with this simple yet

experimentally-constrained method was to provide a chemical mechanism which explains the associations highlighted in the previous sections of this work, by tracking (1) where along a high Sr/Y magmas differentiation path sulphides will precipitate and Cu will decrease, and (2) whether amphibole is responsible for the chemical state change producing the sulphide stabilization and Cu decrease. Similar results could be obtained by using a starting composition for a high Sr/Y, amphibole-producing melt from the literature, feeding that compositions into rhyolite-MELTS, and calculating the evolution of the liquid along a specified P-T path[59]. However, rhyolite-MELTS has limited applicability in wet intermediate systems owing to a lack of precise thermodynamic models for hydrous mafic silicates like amphibole and biotite[59], making our specific model, with an emphasis on amphibole impossible to model using such an approach.

The experimental data used in our model[52] were prepared by manually transcribing Tables 1 (start conditions), Table 2 (model abundances of minerals at each experimental temperature step), and Table 3 (glass and amph compositions, determined by EPMA) into Supplemental Data Table 4. In Ulmer et al. 2018, major elements were the only measured chemical species. Starting abundances of Ni, Cu, Sr, Y, and all REEs were taken from the trace element compositions of the relevant starting materials[40,60,61], and used to model the partitioning of trace elements into fractionating mineral phases following the methods of Shaw 2006[62] (see below) The resulting trace element abundances across each model were treated to the same analysis as the global database for trace element ratios (e.g. Dy/Dy*) and measures of REE curve shapes (e.g. λ). We also calculated SCSS folloowing[27].

To model the trace element abundances of Cu, Ni, Sr, Y, and the REE's found in experimental products of[52], we apply the Rayleigh fractionation equation presented in[62] (Equation 3.20):

$$\frac{c_l^t}{c_o} = F^{D-1}$$

,

where:

t = timestep *t* in a given experiment, corresponding to a specific set of T, P, and X_i conditions. Also called *run number* in ‘ud‘ database.

c_l^t = concentration of an element in the residual liquid

c_o = initial concentration of an element in bulk liquid, before fractionation

F^t = fraction of residual liquid -> $\frac{L}{L_o}$

D^t = "Bulk D," or weighted sum of whole rock partition coefficients, where X_i = mass fraction of mineral *i* in accumulated solid fraction, ad D^{i-l} = : partition coefficient (or K_d) between mineral *i* and liquid *l*:

$$D^t = \sum_{i=0}^{\infty} X_i^t * D_{i-l}^t$$

Final form of equation 3.20 for this model requires us to solve for c_l at each experimental step (run Number) in an experiment, of which there are three experiments total in our experimental database:

$$c_l = c_o * F^{D-1}$$

Sulphide saturation in a melt is described by the experimental parameter, "sulphur content at sulphide saturation," or SCSS[63]. We modeled the SCSS for the experimental products shown in Figure 3 and6 , using the major elements[52] and modeled trace elements (Cu, Ni) of the individual products as inputs using a new SCSS paramterization[27]:

$$\ln\left[\mathrm{S}^{2-}\right]_{\mathrm{SCSS}} = \Delta G^{O}_{FeO-FeS}/\mathrm{RT} + \ln C_{S^{2-}} - \ln a^{silmelt}_{FeO} + \ln a^{Sulf}_{FeS}$$

This method builds on the work of[28], and is very sensitive to the sulphide composition, and Fe-Ni-Cu partioning into that sulphide, as well as P and T at ranges appropriate for our models[27]. SCSS is very sensitive to oxidation state, especially in more evolved andesite[64]. To account for this, we calculated SCSS for a range of S^{6+} speciation end members (0.2, 0.5, and 0.9 in terms of $\frac{S^{6+}}{S_T}$). These are shown schematically in Figure 4, and implications are picked apart in greater detail in the Supplement. The correction for this is taken from[65]:

$$SCSS_{Tot} = \frac{SCSS^{2-}}{\left(1 - \frac{S^{6+}}{\Sigma S}\right)}$$

This in turn is based on an earlier parameterization of S^{6+} as a function of ΔQFM buffer[29]:

$$\frac{S^{6+}}{S_T} = \frac{1}{1 + 10^{(2.1 - 2\Delta FMQ)}}$$

The empirical study we modeled[52] estimated ranges for the fO_2 in terms of ΔNNO oxygen buffer, as between +0.5 and 1.5 for the FC experiments. Taking the equations above, our $\frac{S^{6+}}{S_T}$ ratio should be between **0.89 and 0.07** (this is all fit through an earlier paramterization of $\frac{Fe^{3+}}{Fe^{2+}}$ and fO_2[66]). This is a large range, and shows that oxidation state changes radically throughout the experiments. If we assume the midpoint of this distribution, 0.5 for the sulphate/sulphide ratio, is representative, our correction involves revising up the SCSS a factor of 2 (50%), 1.11 (10%), and 10 (90%) (see Figure 6) to model the effect of different redox conditions on our proposed amphibole control

mechanism on sulphide stability.

4.3.2 Models of Sulphur Content at Sulphide Saturation

The SCSS is negatively correlated with pressure[63] and positively correlated with temperature[28,63,67], melt H_2O content[68], melt FeO, Cu and Ni contents[5,28,635,27,28], and oxygen fugacity (fO_2)[29,67]. For mid-ocean ridge basalts, melt FeO content, oxygen fugacity (fO_2), temperature, and pressure are the main drivers of sulphide saturation[5]. In arc magmas, higher water and sulfur contents[15,69] coupled with higher oxidation state[20,29] cause the SCSS to respond differently as compared to MORB. For most arc magmas, volatile and oxidation conditions lie outside the range for which many SCSS models are calibrated[63], with some exceptions[29,68]. Since most arc magmas have a considerable fraction of sulphur present as S^{6+}, they may instead saturate in anhydrite, which is much more soluble in silicate melts[70].

Like garnet, amphibole is much more stable at high H_2O[52,53,55], but unlike garnet it predominates at moderate depths (20-55 km.[43,44,53]). We have modeled the trace element abundances of experimental results from an existing study to constrain the effect of amphibole on the liquid line of descent in arc magmas, in order to understand how amphibole fractionation may connect major and trace element systematics under high Sr/Y conditions[52]. The experimental study in question ran isobaric experiments under equilibrium (EC) and fractional crystallization (FC) conditions at 1.0 GPa on hydrous basaltic[61] and andesitic melts[6052]. Given the mineral proportions and glass compositions reported from[52], we modeled the effect of phases like amphibole on SCSS, major, and trace element abundances as they appear on the liquidus (Figure 6, symbolized curves in Figure 3, orange field in Figure 5). Additional analysis of the effect of amphibole fractionation on melt Mg# show that amphibole is more than capable of moderating calc-alkaline differentiation, as Mg# decreases con-

sistently across the amphibole stability boundary (see Supporting Information Figure 10). This is in agreement with the bulk major element control ascribed to amphibole in high pressure experiments[52,53]. These modeled effects of amphibole can be compared to generic differentiation trends in major elements and Cu (Figure 3) to determine the specific process that is driving Cu depletion across all subduction zones. In order to develop the model, we applied a simple fractional crystallization model following[62] for the trace elements Cu, Ni, Sr, Y, and all REEs (model details in Supporting Information).

We used the major element glass compositions produced at each step of the experiments to model SCSS using the equations of[27], which relates SCSS to the FeO, MgO, Cu and Ni melt contents, and temperature (Methods). For all experiments, SCSS decreases with FeO and decreasing temperature (Figure 6a and 6b respectively)[63]. The SCSS values are initially calculated assuming the redox state of the magma will favor mainly S^{2-}[27]. To correct for this in the more oxidized experimental runs[52], we used an S^{6+} correction[65] (see Methods for details) to determine realistic SCSS curves for more oxidized arc magmas, at S^{6+} proportions of 10, 50, and 90% of total sulphur (green curves with different symbols in Figure 6a, 6b). We mark the onset of amphibole crystallization in each run and its effect on whole rock FeO concentration using grey boxes. High-temperature (>1050 °C) FeO loss is attributed to clinopyroxene, followed by a much more dramatic lowering of SCSS at amphibole-in. These two FeO loss trends are separated by an abrupt decrease in SCSS, which is a function of temperature change as clinopyroxene abundance decreases and amphibole starts to appear (blue curve in Figure 6a). The onset of amphibole fractionation is associated with a dramatic lowering of the SCSS (Figure 6a). We infer that amphibole is the most important mineral phase in our model, as clinopyroxene in these models only fractionates at temperatures greater than 1050 °C. Since

arc magmas usually contain bulk sulphur contents of $>$ 1000 ppm (red line in Figures 6a and 6b)[69], these models confirm that most hydrous arc magmas are at or near sulphide saturation[20] during differentiation, and as a result will become depleted in Cu as sulphides are removed. The presence of sulphides in magmas has been reported by an increasing number of studies, in areas as diverse as Western North America[48], Kīlauea[65], the Ecuadorian Andes[71], and even sulphide-rich hornblende cumulate xenoliths[21,72].

Even accounting for the uncertainty in the oxidation state of the magmas that produced the whole rocks in the global database, there is compelling evidence that amphibole fractionation drives cal-alkaline differentiation, extensive sulphide fractionation, and subsequent melt [Cu] depletion. Another Fe-rich mineral, magnetite, has been implicated in taking up substantial quantities of Fe^{3+}, which has been shown to lead to reduction of S from S^{6+} to S^{2-}. Since sulphide saturates at much lower [S] as compared to sulphate[13], like our oxidized andesite models, higher proportions of S^{2-} will promote sulphide fractionation and metal loss. The crucial difference is that amphibole's ability to promote sulphide fractionation and Cu loss is due to its reduction of total melt [FeO], as opposed to models involving the fractionation of high $Fe_3{}^+/Fe_{tot}$ phases like magnetite.

Global Controls on Copper in Arc Volcanic Rocks

Our analysis of the global database demonstrates that amphibole fractionation, accepted as a driver of high Sr/Y signals[22,23,30], can promote sulphide fractionation via Fe-loss and consequent Cu depletion in a typical calc-alkaline magma. We anticipate that the sulphide concerned is crystalline sulphide (e.g. monosulphide solid solution; MSS) which should predominate in the lower temperature conditions of an arc magmas as compared to MORB[10,72–74]. An important con-

sideration we need to make in posing this model is whether there is direct evidence linking MSS fractionation with Cu depletion in arc magmatic sequences. We attempt to provide such evidence by analyzing those whole rock compositions in ArcMetals that can be shown to have fractionated sulphide. In Figure 7, we plot whole rock Cu/Ag vs. MgO , coloured for both Gd/Yb (Figure 7a), Dy/Dy* (Figure 7b), and for crustal thickness (CT) (Figure 7c). The motivation behind constructing such plots stem from the fact that Cu fractionates more strongly into MSS than Ag[6], and such a ratio gives us the benefit of sensitively detecting the presence of a fractionating MSS at sulphide saturation[46]. A low Cu/Ag ratio, below average mid-ocean ridge basalt (MORB)[46,75] and continental crust[76], is consistent with crystalline sulphide fractionation and consequent Cu removal from the silicate melt[46]. Gd/Yb (Figure 7a) is a proxy for garnet involvement in petrogenesis because Gd partitions less strongly into garnet than Yb[75], and has been used to infer the prevalence of garnet fractionation in the Andes[54].

The highest Gd/Yb ratios are associated with whole rocks with the lowest Cu/Ag for a given MgO content (Figure 7a), suggesting a direct correlation between the proportion of garnet fractionation and the proportion of sulfide fractionation. Owing to the complexities in analysing whole rocks for Ag, Cu/Ag datasets are rare and are currently biased towards the Andes data, though there are some measurements in other transitional arcs (Figure 7 symbols). There is no clear link between Cu/Ag in the whole rock and crustal thickness, but the very thickest crust (>40 km) is associated with evolved volcanic rocks with in general a high Gd/Yb (indicating garnet in the source or garnet fractionation) and low Cu/Ag. Figure 7b shows that lower Dy/Dy*, indicative of amphibole, is also associated with low Cu/Ag, evolved magmas. Thus, both garnet and amphibole are implicated in the petrogenesis of magmas that have experienced the

most sulphide fractionation. One drawback to using Cu/Ag as a proxy for sulphides in our global database is the dearth of available Ag and other chalcophile data in the literature. Only in the past 5-10 years have Ag and other difficult to measure elements become easily measurable using ICPMS[46,49,54,65,77]. As studies reporting suites of chalcophile elements in magmatic systems grow, future iterations of this database may yet be able to make broader, more detailed analysis of Cu/Ag in arc systems.

Our schematic model (Figure 8) emphasizes the primary importance of amphibole fractionation, and the secondary importance of garnet fractionation and garnet[19] in the mantle source. We emphasize the importance of amphibole as a universal petrological mechanism that explains many of the generic features of high ore-potential magmas. The global applicability of our amphibole-centred model complements garnet fractionation models, which work best in arcs with mature magmatic columns, deep brittle-ductile transitions (which promote longer residence times of magma in crust[19]), and thicker crusts[19,54], and even magnetite fractionation models, which work best in young island arcs and/or back-arc basins[13,75]. We see our amphibole-centered model on a continuum with these other petrological models, where water-rich, calc-alkaline trending arc magmas stored in the deep crust (15-50 km.) will fractionate amphibole to stabilize sulphide in moderately thick oceanic to transitional arcs. As these arcs evolve, garnet will fill much the same role as amphibole in controlling Fe and stabilizing sulphide. This allows for a certain degree of temporal evolution in the primary petrological vector controlling bulk [Cu] in arc magmas, where we would expect a young arc to modulate its Cu via magnetite[13], evolving to amphibole at a moderate maturity an thickness, culminating in garnet fractionation dominated Cu control by the time the arc reaches maturity[19].

One point of departure with our analysis from some work in the literature

regards the importance of the timing of sulphide saturation. Some previous studies[19] have implicitly assumed that early sulphide saturation is detrimental to eventual porphyry copper deposit development, articulating the 'Cu paradox,' of low magmatic [Cu] being associated with ore deposits[19]. Studies using platinum group elements as proxies for sulphide saturation in arc systems make this assumption explicit, arguing that ore development requires late sulphide saturation[12]. However, as suggested in recent work[21], porphyry systems that have experienced both prolonged amphibole fractionation and early sulphide crystallization (and subsequent Cu loss) seem perfectly capable of developing porphyry deposits later in their lifetime[21]. Our global analysis confirms that melt Cu concentration does not act as a primary control on porphyry fertility. In agreement with the observation that high Sr/Y magmas have lower Cu concentrations[19,20] (Figure 3c), our analysis finds that combined amphibole and/or garnet fractionation can lead directly to early sulphide saturation (Figure 6). The low magmatic Cu concentrations we observe in the high Sr/Y magmas in our database are thus reflective of important processes like amphibole fractionation that are generating magmas that may be capable of forming ores.

5 Conclusion

In this study we present a comprehensive geochemical and geophysical database of volcanic whole rock samples across 17 arcs covering most of the Earth's active subduction zones. This database, ArcMetals, is differentiated from previous efforts by a rigorous filtration and data compilation strategy. Here we present the first order features of this global dataset alongside a simple trace element and sulphide saturation model to identify the key petrological processes that control [Cu] in arc magmas. High Sr/Y magmas show geochemical evidence for hav-

ing been generated in hydrous, possibly garnet-bearing, mantle wedges. More importantly, there is a strong association between high Sr/Y, calc-alkaline differentiation, and amphibole +/- garnet fractionation. High Sr/Y magmas show depletion of Fe during calc-alkaline differentiation and are associated with significantly lower whole rock mean Cu concentrations and thicker continental crust. These trends are driven by extensive amphibole fractionation, which lowers melt Fe contents and hence SCSS, driving sulphide saturation and Cu removal into sulphides. In conjunction with this, the hydrous composition of the source region could promote the stabilization of garnet in the mantle source, while high water contents in a high pressure magma could promote both amphibole and garnet fractionation. As has been shown in previous work, we contend that garnet fractionation can also contribute to Fe depletion, and subsequently increases the likelihood of sulphide saturation at greater depths before amphibole fractionates[19,54]. However, garnet fractionation is restricted to high pressures and may not occur in all arcs[19]. This question of prevalence emphasizes that our preferred petrological vector, amphibole, provides a generic explanation for global Cu systematics, as any arc magma with enough water will fractionate amphibole at intermediate compositions. Importantly, our analysis indicates that amphibole fractionation is, irrespective of the presence of garnet on the liquidus, capable of lowering SCSS and promoting early sulphide saturation. Magmatic Cu contents are thus reflective of the crucial petrological processes identified in our global database and are not a driver or proxy for ore fertility.

While many arc magmas fractionate amphibole[43] and most (if not all) arc magmas are rich in water and other volatiles, porphyry deposits remain rare. Our study demonstrates early sulphide saturation is not necessarily detrimental to later porphyry formation from a typical calc-alkaline arc magmas. Even more crucial to this process is the tectonic (e.g. compressional stresses), geodynamic,

geological, and temporal conditions of the magma reservoir system itself[21,23,78], which along with the geochemical factors analyzed here, strongly influence whether or not a porphyry system will form. It is possible that porphyry mineralization requires long timescales for differentiation and fluid segregation[23,78] under conducive crustal configurations, which could promote further amphibole crystallization in a melt-rich mid-crustal hot zone[78]. Larger magma volumes may be optimal for achieving extreme volatile concentration[79] (e.g. minimum 1000 km^3 for Bingham Canyon and other large porphyry deposits[25,78]), which would also favor porphyry mineralization[21,23,24,78].

References

1. Arndt, N. T. *et al.* Future global mineral resources. *Geochemical Perspectives* **6,** 1–171 (2017).

2. Singer, D. A., Berger, V. I., Menzie, W. D. & Berger, B. R. Porphyry copper deposit density. *Economic Geology* **100,** 491–514 (2005).

3. Hedenquist, J. W. & Lowenstern, J. B. The role of magmas in the formation of hydrothermal ore deposits. *Nature* **370,** 519–527. ISSN: 0028-0836. http://www.nature.com/doifinder/10.1038/370519a0 (Aug. 1994).

4. Kiseeva, E. S. & Wood, B. J. A simple model for chalcophile element partitioning between sulphide and silicate liquids with geochemical applications. *Earth and Planetary Science Letters.* ISSN: 0012821X (2013).

5. Kiseeva, E. S., Fonseca, R. O. & Smythe, D. J. Chalcophile elements and sulfides in the upper mantle. *Elements* **13,** 111–116 (2017).

6. Patten, C., Barnes, S.-J., Mathez, E. A. & Jenner, F. E. Partition coefficients of chalcophile elements between sulfide and silicate melts and

the early crystallization history of sulfide liquid: LA-ICP-MS analysis of MORB sulfide droplets. *Chemical Geology* **358,** 170–188 (2013).

7. Jugo, P., Candela, P. & Piccoli, P. Magmatic sulfides and Au: Cu ratios in porphyry deposits: an experimental study of copper and gold partitioning at 850 C, 100 MPa in a haplogranitic melt–pyrrhotite–intermediate solid solution–gold metal assemblage, at gas saturation. *Lithos* **46,** 573–589 (1999).

8. Simon, A. C., Pettke, T., Candela, P. A., Piccoli, P. M. & Heinrich, C. A. Copper partitioning in a melt–vapor–brine–magnetite–pyrrhotite assemblage. *Geochimica et Cosmochimica Acta* **70,** 5583–5600 (2006).

9. Li, Y. & Audétat, A. Effects of temperature, silicate melt composition, and oxygen fugacity on the partitioning of V, Mn, Co, Ni, Cu, Zn, As, Mo, Ag, Sn, Sb, W, Au, Pb, and Bi between sulfide phases and silicate melt. *Geochimica et Cosmochimica Acta.* ISSN: 00167037 (2015).

10. Li, Y. & Audétat, A. Gold solubility and partitioning between sulfide liquid, monosulfide solid solution and hydrous mantle melts: Implications for the formation of Au-rich magmas and crust–mantle differentiation. *Geochimica et Cosmochimica Acta* **118,** 247–262 (2013).

11. Wilkinson, J. J. Triggers for the formation of porphyry ore deposits in magmatic arcs. *Nature Geoscience* **6,** 917. http://dx.doi.org/10.1038/ngeo1940%20http://10.0.4.14/ngeo1940%20https://www.nature.com/articles/ngeo1940#supplementary-information (Oct. 2013).

12. Park, J.-W. *et al.* Chalcophile element fertility and the formation of porphyry Cu±Au deposits. *Mineralium Deposita* **54,** 657–670 (2019).

13. Jenner, F. E., ONeill, H. S. C., Arculus, R. J. & Mavrogenes, J. A. The magnetite crisis in the evolution of arc-related magmas and the initial

concentration of Au, Ag and Cu. *Journal of Petrology.* ISSN: 00223530 (2010).

14. Chiaradia, M. Copper enrichment in arc magmas controlled by overriding plate thickness. *Nature Geoscience* **7,** 43–46 (2014).

15. Edmonds, M. & Mather, T. A. Volcanic sulfides and outgassing. *Elements.* ISSN: 18115217 (2017).

16. Blundy, J., Mavrogenes, J., Tattitch, B., Sparks, S. & Gilmer, A. Generation of porphyry copper deposits by gas–brine reaction in volcanic arcs. *Nature Geoscience* **8,** 235–240 (2015).

17. Nadeau, O., Williams-Jones, A. E. & Stix, J. Sulphide magma as a source of metals in arc-related magmatic hydrothermal ore fluids. *Nature Geoscience.* ISSN: 17520894 (2010).

18. Audetat, A., Pettke, T., Heinrich, C. A. & Bodnar, R. J. Special paper: the composition of magmatic-hydrothermal fluids in barren and mineralized intrusions. *Economic Geology* **103,** 877–908 (2008).

19. Lee, C.-T. A. & Tang, M. How to make porphyry copper deposits. *Earth and Planetary Science Letters* **529,** 115868 (2020).

20. Richards, J. P. The oxidation state, and sulfur and Cu contents of arc magmas: implications for metallogeny. *Lithos* **233,** 27–45 (2015).

21. Du, J. & Audétat, A. Early sulfide saturation is not detrimental to porphyry Cu-Au formation. *Geology* **48,** 519–524 (2020).

22. Richards, J. P. Magmatic to hydrothermal metal fluxes in convergent and collided margins. *Ore Geology Reviews* **40,** 1–26 (2011).

23. Loucks, R. Distinctive composition of copper-ore-forming arcmagmas. *Australian Journal of Earth Sciences* **61,** 5–16 (2014).

24. Rezeau, H. & Jagoutz, O. The importance of H2O in arc magmas for the formation of porphyry Cu deposits. *Ore Geology Reviews,* 103744 (2020).

25. Chelle-Michou, C., Rottier, B., Caricchi, L. & Simpson, G. Tempo of magma degassing and the genesis of porphyry copper deposits. *Scientific reports* **7,** 40566 (2017).

26. Steinberger, I., Hinks, D., Driesner, T. & Heinrich, C. A. Source plutons driving porphyry copper ore formation: combining geomagnetic data, thermal constraints, and chemical mass balance to quantify the magma chamber beneath the Bingham Canyon deposit. *Economic Geology* **108,** 605–624 (2013).

27. O'Neill, H. The thermodynamic controls on sulfide saturation in silicate melts with application to Ocean Floor Basalts. (2020).

28. Smythe, D. J., Wood, B. J. & Kiseeva, E. S. The S content of silicate melts at sulfide saturation: new experiments and a model incorporating the effects of sulfide composition. *American Mineralogist* **102,** 795–803 (2017).

29. Jugo, P. J., Wilke, M. & Botcharnikov, R. E. Sulfur K-edge XANES analysis of natural and synthetic basaltic glasses: Implications for S speciation and S content as function of oxygen fugacity. *Geochimica et Cosmochimica Acta* **74,** 5926–5938 (2010).

30. Chiaradia, M. Crustal thickness control on Sr/Y signatures of recent arc magmas: an Earth scale perspective. *Scientific reports* **5,** 8115 (2015).

31. Farner, M. J. & Lee, C.-T. A. Effects of crustal thickness on magmatic differentiation in subduction zone volcanism: a global study. *Earth and Planetary Science Letters* **470,** 96–107 (2017).

679 32. Sarbas, B. & Nohl, U. The GEOROC database as part of a growing geoin-
680 formatics network. *Geoinformatics* (2008).

681 33. Hayes, G. P. *et al.* Slab2, a comprehensive subduction zone geometry
682 model. *Science* **362,** 58–61 (2018).

683 34. Szwillus, W., Afonso, J. C., Ebbing, J. & Mooney, W. D. Global crustal
684 thickness and velocity structure from geostatistical analysis of seismic data.
685 *Journal of Geophysical Research: Solid Earth* **124,** 1626–1652 (2019).

686 35. Pasyanos, M. E., Masters, T. G., Laske, G. & Ma, Z. LITHO1. 0: An
687 updated crust and lithospheric model of the Earth. *Journal of Geophysical*
688 *Research: Solid Earth* **119,** 2153–2173 (2014).

689 36. Syracuse, E. M. & Abers, G. A. Global compilation of variations in slab
690 depth beneath arc volcanoes and implications. *Geochemistry, Geophysics,*
691 *Geosystems.* ISSN: 15252027 (2006).

692 37. Richards, J. P. High Sr/Y ratio magmas and porphyry Cu, Mo, Au De-
693 posits:Just add water. *Economic Geology* **106,** 1075–1081. ISSN: 0361-0128.
694 http://dx.doi.org/10.2113/econgeo.106.7.1075 (Nov. 2011).

695 38. Ewart, A. & Griffin, W. Application of proton-microprobe data to trace-
696 element partitioning in volcanic rocks. *Chemical Geology* **117,** 251–284
697 (1994).

698 39. Green, T. H. Experimental studies of trace-element partitioning applicable
699 to igneous petrogenesis—Sedona 16 years later. *Chemical Geology* **117,** 1–
700 36 (1994).

701 40. Grove, T., Parman, S., Bowring, S., Price, R. & Baker, M. The role of an H
702 2 O-rich fluid component in the generation of primitive basaltic andesites
703 and andesites from the Mt. Shasta region, N California. *Contributions to*
704 *Mineralogy and Petrology* **142,** 375–396 (2002).

41. Stolper, E. Water in silicate glasses: an infrared spectroscopic study. *Contributions to Mineralogy and Petrology* **81,** 1–17 (1982).

42. Foden, J. & Green, D. Possible role of amphibole in the origin of andesite: some experimental and natural evidence. *Contributions to Mineralogy and Petrology* **109,** 479–493 (1992).

43. Ridolfi, F., Renzulli, A. & Puerini, M. Stability and chemical equilibrium of amphibole in calc-alkaline magmas: an overview, new thermobarometric formulations and application to subduction-related volcanoes. *Contributions to Mineralogy and Petrology* **160,** 45–66 (2010).

44. Santana, L. V., McLeod, C., Blakemore, D., Shaulis, B. & Hill, T. Bolivian hornblendite cumulates: Insights into the depths of Central Andean arc magmatic systems. *Lithos,* 105618 (2020).

45. Lee, C.-T. A. *et al.* Copper systematics in arc magmas and implications for crust-mantle differentiation. *Science* **336,** 64–68 (2012).

46. Jenner, F. E. Cumulate causes for the low contents of sulfide-loving elements in the continental crust. *Nature Geoscience.* ISSN: 17520908 (2017).

47. Davidson, J., Turner, S. & Plank, T. Dy/Dy*: variations arising from mantle sources and petrogenetic processes. *Journal of Petrology* **54,** 525–537 (2013).

48. Chen, K. *et al.* Sulfide-bearing cumulates in deep continental arcs: The missing copper reservoir. *Earth and Planetary Science Letters,* 115971 (2019).

49. Cox, D., Watt, S. F., Jenner, F. E., Hastie, A. R. & Hammond, S. J. Chalcophile element processing beneath a continental arc stratovolcano. *Earth and Planetary Science Letters* **522,** 1–11 (2019).

730 50. O'Neill, H. S. C. The smoothness and shapes of chondrite-normalized rare
731 earth element patterns in basalts. *Journal of Petrology* **57,** 1463–1508
732 (2016).

733 51. Sullivan, L. *Hypothesis Testing - Analysis of Variance (ANOVA)* https://
734 sphweb.bumc.bu.edu/otlt/MPH-Modules/BS/BS704_HypothesisTesting-
735 ANOVA/BS704_HypothesisTesting-Anova_print.html.

736 52. Ulmer, P., Kaegi, R. & Müntener, O. Experimentally derived intermediate
737 to silica-rich arc magmas by fractional and equilibrium crystallization at
738 1· 0 GPa: An evaluation of phase relationships, compositions, liquid lines
739 of descent and oxygen fugacity. *Journal of Petrology* **59,** 11–58 (2018).

740 53. Alonso-Perez, R., Müntener, O. & Ulmer, P. Igneous garnet and amphibole
741 fractionation in the roots of island arcs: experimental constraints on an-
742 desitic liquids. *Contributions to Mineralogy and Petrology* **157,** 541 (2009).

743 54. Cox, D. *et al.* Elevated magma fluxes deliver high-Cu magmas to the upper
744 crust. *Geology* **48** (2020).

745 55. Greene, A. R., DeBARI, S. M., Kelemen, P. B., Blusztajn, J. & Clift, P. D.
746 A detailed geochemical study of island arc crust: the Talkeetna arc section,
747 south–central Alaska. *Journal of Petrology* **47,** 1051–1093 (2006).

748 56. Bissig, T., Leal-Mejia, H., Stevens, R. B. & Hart, C. J. High Sr/Y magma
749 petrogenesis and the link to porphyry mineralization as revealed by Garnet-
750 Bearing I-type granodiorite porphyries of the Middle Cauca Au-Cu Belt,
751 Colombia. *Economic Geology* **112,** 551–568 (2017).

752 57. Ducea, M. N., Saleeby, J. B. & Bergantz, G. The architecture, chemistry,
753 and evolution of continental magmatic arcs. *Annual Review of Earth and*
754 *Planetary Sciences* **43,** 299–331 (2015).

58. Feigenson, M. D. & Carr, M. J. The source of Central American lavas: inferences from geochemical inverse modeling. *Contributions to Mineralogy and Petrology* **113,** 226–235 (1993).

59. Gualda, G. A., Ghiorso, M. S., Lemons, R. V. & Carley, T. L. Rhyolite-MELTS: a modified calibration of MELTS optimized for silica-rich, fluid-bearing magmatic systems. *Journal of Petrology* **53,** 875–890 (2012).

60. Baker, M. B., Grove, T. L. & Price, R. Primitive basalts and andesites from the Mt. Shasta region, N. California: products of varying melt fraction and water content. *Contributions to Mineralogy and Petrology* **118,** 111–129 (1994).

61. Hürlimann, N. *et al.* Primary magmas in continental arcs and their differentiated products: petrology of a post-plutonic dyke suite in the Tertiary Adamello batholith (Alps). *Journal of Petrology* **57,** 495–534 (2016).

62. Shaw, D. M. *et al. Trace elements in magmas: a theoretical treatment* (Cambridge University Press, 2006).

63. O'Neill, H. & Mavrogenes, J. A. The sulfide capacity and the sulfur content at sulfide saturation of silicate melts at 1400 C and 1 bar. *Journal of Petrology* **43,** 1049–1087 (2002).

64. Jugo, P. J. Sulfur content at sulfide saturation in oxidized magmas. *Geology* **37,** 415–418 (2009).

65. Wieser, P., Jenner, F., Edmonds, M., Maclennan, J. & Kunz, B. Chalcophile elements track the fate of sulfur at Kilauea Volcano, Hawai'i (2020).

66. Kress, V. C. & Carmichael, I. S. The compressibility of silicate liquids containing Fe 2 O 3 and the effect of composition, temperature, oxygen fugacity and pressure on their redox states. *Contributions to Mineralogy and Petrology* **108,** 82–92 (1991).

781 67. Nash, W. M., Smythe, D. J. & Wood, B. J. Compositional and tempera-
782 ture effects on sulfur speciation and solubility in silicate melts. *Earth and*
783 *Planetary Science Letters* **507,** 187–198. ISSN: 0012-821X. http://www.
784 sciencedirect.com/science/article/pii/S0012821X18307155 (2019).

785 68. Fortin, M.-A., Riddle, J., Desjardins-Langlais, Y. & Baker, D. R. The effect
786 of water on the sulfur concentration at sulfide saturation (SCSS) in natural
787 melts. *Geochimica et Cosmochimica Acta* **160,** 100–116 (2015).

788 69. Wallace, P. J. & Edmonds, M. The sulfur budget in magmas: evidence from
789 melt inclusions, submarine glasses, and volcanic gas emissions. *Reviews in*
790 *Mineralogy and Geochemistry* **73,** 215–246 (2011).

791 70. Zajacz, Z. & Tsay, A. An accurate model to predict sulfur concentration at
792 anhydrite saturation in silicate melts. *Geochimica et Cosmochimica Acta*
793 **261,** 288–304 (2019).

794 71. Georgatou, A., Chiaradia, M., Rezeau, H. & Wälle, M. Magmatic sulphides
795 in Quaternary Ecuadorian arc magmas. *Lithos* **296,** 580–599 (2018).

796 72. Chang, J. & Audétat, A. Petrogenesis and metal content of hornblende-rich
797 xenoliths from two Laramide-age magma systems in southwestern USA:
798 insights into the metal budget of arc magmas. *Journal of Petrology* **59,**
799 1869–1898 (2018).

800 73. Keith, M., Haase, K. M., Klemd, R., Schwarz-Schampera, U. & Franke,
801 H. Systematic variations in magmatic sulphide chemistry from mid-ocean
802 ridges, back-arc basins and island arcs. *Chemical Geology.* ISSN: 00092541
803 (2017).

804 74. Rottier, B., Audétat, A., Koděra, P. & Lexa, J. Origin and Evolution of
805 Magmas in the Porphyry Au-mineralized Javorie Volcano (Central Slo-

vakia): Evidence from Thermobarometry, Melt Inclusions and Sulfide Inclusions. *Journal of Petrology* **60,** 2449–2482 (2019).

75. Jenner, F. E. *et al.* Chalcophile element systematics in volcanic glasses from the northwestern Lau Basin. *Geochemistry, Geophysics, Geosystems.* ISSN: 15252027 (2012).

76. Holland, H. D. & Turekian, K. K. Treatise on geochemistry (2004).

77. Jenner, F. E. & Arevalo, R. D. Major and trace elerment analysis of natural and experimental igneous systems using LA-ICP-MS. *Elements.* ISSN: 18115217 (2016).

78. Chiaradia, M. & Caricchi, L. Stochastic modelling of deep magmatic controls on porphyry copper deposit endowment. *Scientific reports* **7,** 1–11 (2017).

79. Rohrlach, B. D., Loucks, R. R. & Porter, T. Multi-million-year cyclic ramp-up of volatiles in a lower crustal magma reservoir trapped below the Tampakan copper-gold deposit by Mio-Pliocene crustal compression in the southern Philippines. *Super porphyry copper and gold deposits: A global perspective* **2,** 369–407 (2005).

Data Availability

All of our data, code, and protocols are available at the corresponding author's GitHub: https://github.com/ndb38/slab_metals. This current link is subject to change: the database and all associated code is going to be stream lined into a less crowded repository in future versions, and allowed to virtually run through Binder. The code and figures will be updated in future versions of the database, but all the material pertaining to this paper will be preserved.

Acknowledgements

We thank Callum Reekie for providing the Python code for the SCSS models, and for useful comments on SCSS. We thank Penny Wieser for providing a critical appraisal of our early database, and helpful comments regarding the SCSS and trace elements models and their outputs. An additional thank you is extended to James Crosby and Andrew Whyte for their early comments on the importance of amphibole. We would also like to thank Cin-Ty Lee, and two anonymous reviewers for their constructive comments on an earlier version of this manuscript. We would also like to thank the attendees of Goldschmidt 2020 for their constructive and supportive comments. We acknowledge funding from the NERC Centre for the Observation and Modelling of Earthquakes, Volcanoes and Tectonics (COMET). The Gates Cambridge Trust provides financial support for NDB's PhD.

Author Contributions

NDB conceived the project with advice and comments from ME and FJ. NDB compiled the database, wrote the Python code, and performed the analysis. ME., FJ, AA, and HW provided equal contributions regarding data interpretations and significant references. NDB wrote the manuscript with equal editing contributions from ME, FJ, AA, and HW.

Competing Interests

The authors declare no competing interests.

Materials and Correspondence

All correspondence should be directed to Nicholas Barber (ndb38@cam.ac.uk).

Figures

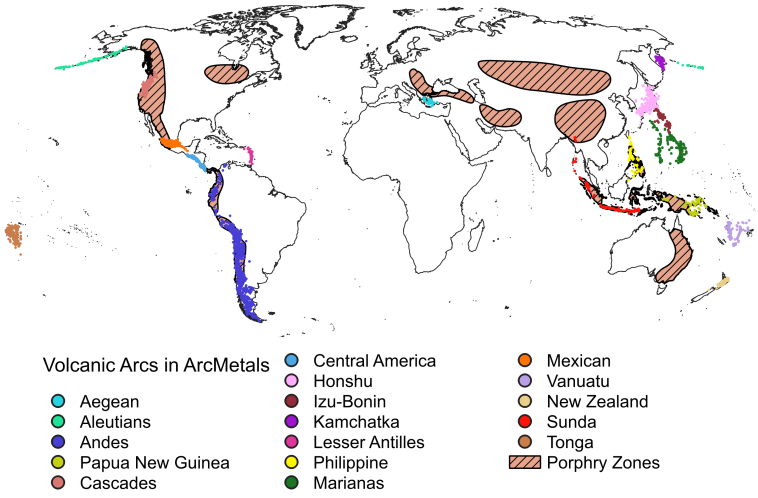

Figure 1: Global distribution of samples used in ArcMelts2, our global data compilation. Sample locations are color coded by arc. Samples are overlayed on zones of porphyry mineralization, taken from [2]. Created using QGIS 3.10.

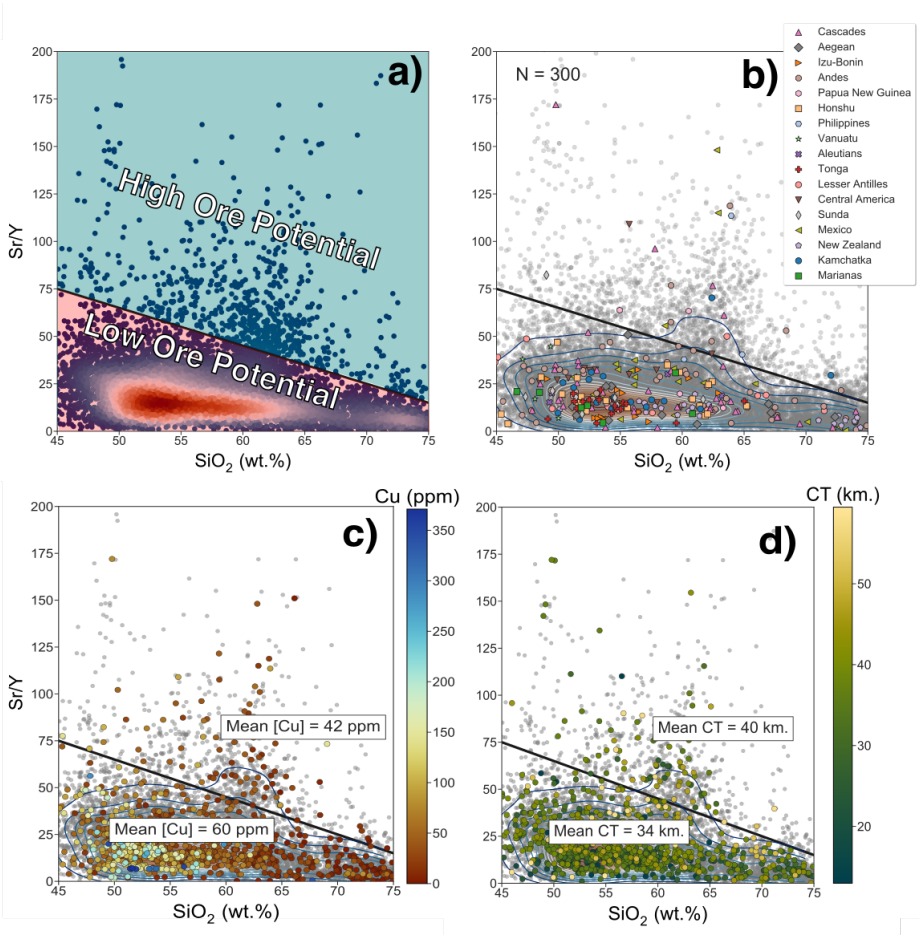

Figure 2: Sr/Y vs. SiO_2 plots, colored for different features. Plots b) and c) are both sub-sampled to only display 300 (b) and 1000 (c) samples for visual clarity. The black line called out in a) differentiates "high" from "low" ore potential, as defined in the literature [23]. Magmas sitting above the black line have higher ore formation potential. Plot a) is colored by the density of points in the total dataset, and contours for sample density are included in all subsequent plots. Plot b) shows a sub-sample of arc magmas colored and symbolized by arc; notice how ore-producing arcs are the only ones that tend to proliferate above the high ore potential line. Plot c) shows a sub-sample of the database colored for Cu, where high and low ore potential magmas have mean [Cu] of 42 and 60 respectively. Similarly, plot d) shows that high ore potential magmas have thicker crust, on average, than low ore potential magmas

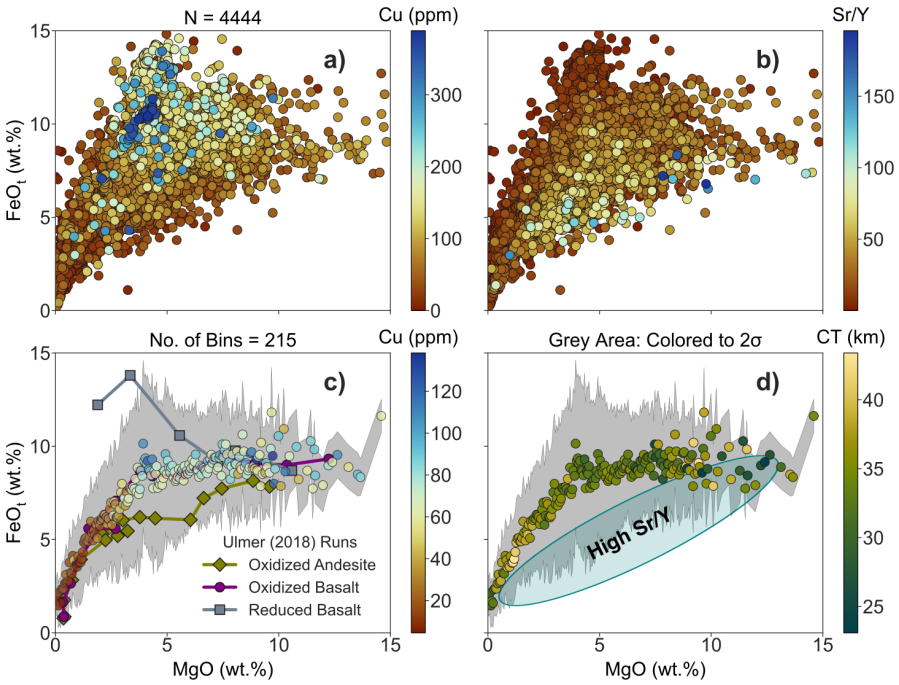

Figure 3: Differentiation trends for the entire dataset, colored for Cu in a) and Sr/Y in b). The highest Cu and Sr/Y measurements are ordered to plot on top of lower measurements. In (c) and (d), resampled averages are calculated for the full database (N = < 12,000) every 0.05 wt.% of MgO, colored for c) Cu (ppm) and d) Crust Thickness (km.). Errors colored out to 2σ, smoothed by a factor of 1.5 to reduce observed spread. Superimposed on the global database (c) are the empirical results of fractional crystallization experiments in arc conditions from [52]. Like Figure 5, blue ellipse is the area where high Sr/Y magmas plot in this Figure (5d)

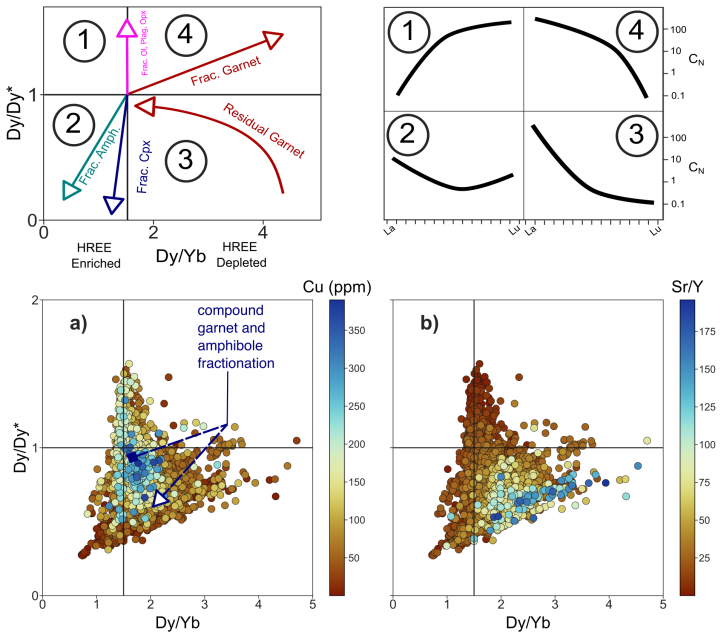

Figure 4: Panels showing the distribution of a) Cu and b) Sr/Y in Dy/Dy vs. Dy/Yb space. These Dy plots show relative fractionation trends according to which mineral phase is dominant. The starting point of each schematic mineral vector is in reference to a chrondrite normalized REE composition. The lowest Cu and highest Sr/Y magmas sit in an area generated by a combination of amphibole and garnet fractionation, and potential mantle source garnet melting. Points in a) and b) are ordered highest to lowest, with the highest Cu and Sr/Y stacked on top. Also shown as a blue ellipse is the area where high Sr/Y magmas plot in Dy/Dy* vs. Dy/Yb space. The dark blue arrow in plot a) shows the expected differentiation path of a magma ascending from high to low pressure, and experiencing first garnet, then amphibole fractionation. Such a liquid line of descent (LLD) can explain the spread in our high ore potential field.

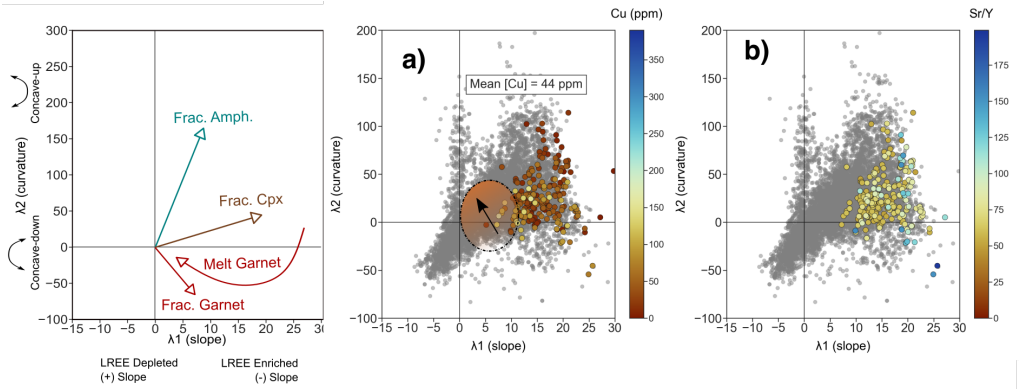

Figure 5: REE behaviour as described by λ spider-plot shape parameters [50]. Top panels are schematics, showing how $\lambda 1$ vs. $\lambda 2$ plots describe mineralogical controls on REE's during differentiation. While $\lambda 1$ describes slope, it is calculated according to the radius of ordered REEs. Hence, a negative $\lambda 1$ corresponds to a positively sloped REE spider profile. a) and b) plot $\lambda 1$ vs. $\lambda 2$ colored for Cu and Sr/Y respectively. Grey points show the entire global database. Colored points are those that plot in the high ore potential field of Figure 3. Mean [Cu] of high Sr/Y field given in a). Empirical results from [52] are shown in the orange shaded area in Figur a) and b), where the arrow denotes the evolving REE contents of empirical products in λ space.

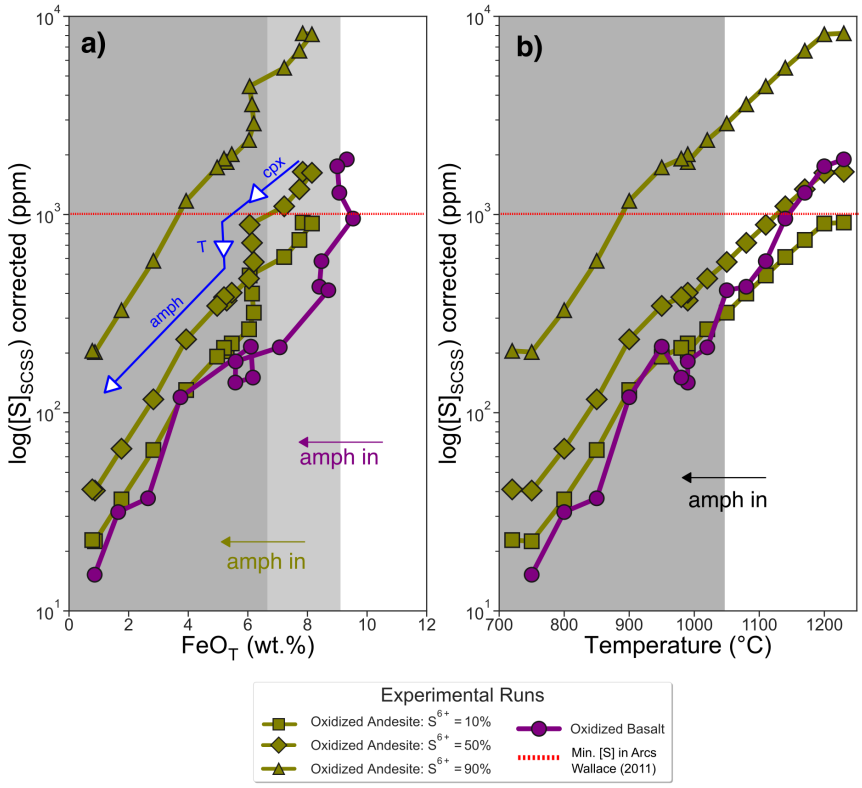

Figure 6: Empirical results of glasses from [52], using initial trace element abundances from [40, 60, 61], and the SCSS model of [27]. Plots show log(SCSS) vs. a) Total FeO and b) c) log(SCSS) vs. Temperature °C. Starting materials in each run were symbolized as: olive colored diamonds = oxidized andesite; purple circles = oxidized basalt;. Vertical grey bars indicate the onset of amphibole fractionation for the oxidized andesite vs. the oxidized basalt runs, respectively. Amphibole is measured to appear around 6.5 wt.% FeO and 1050 °C). SCSS of the model andesite was reported for 3 proportions of $S^{6+}/\Sigma S$ - 10% (squares), 50% (diamonds), and 90% (triangles) respectively, following the corrections in [65]. The red dashed line at 1000 ppm [S] is the average minimum [S] content in arc magmas, taken from [69]. Discussion of partition coefficients used to model SCSS, Cu, and Sr/Y can be found in the Methods and Supporting Information.)

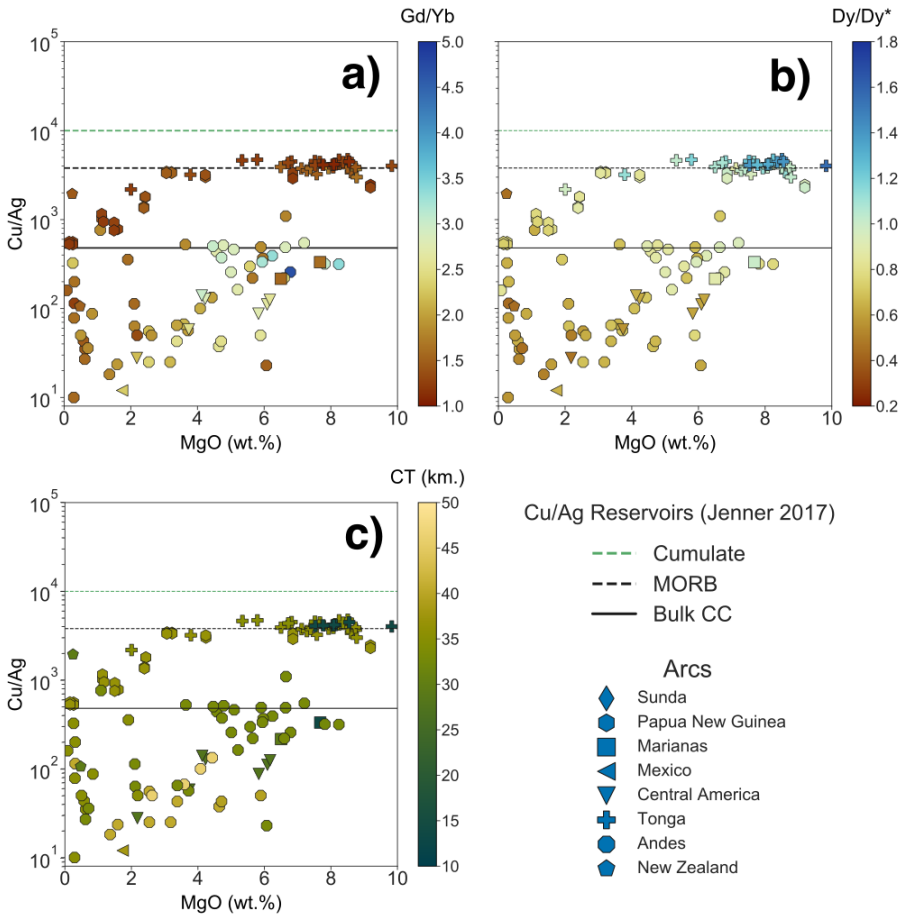

Figure 7: Cu/Ag (as a proxy for crystalline sulphide fractionation) plotted against MgO. Colored for a) Gd/Yb, b) Dy/Dy*, and c) Crust Thickness. Majority of samples plotted here are whole rock compositions. Individual samples are symbolized according to the arc they come from. Plot structure and reference lines for Cu/Ag adapted from [46], as are the reference compositions for Cu/Ag in Sulphide cumulates, MORB, and Bulk CC.

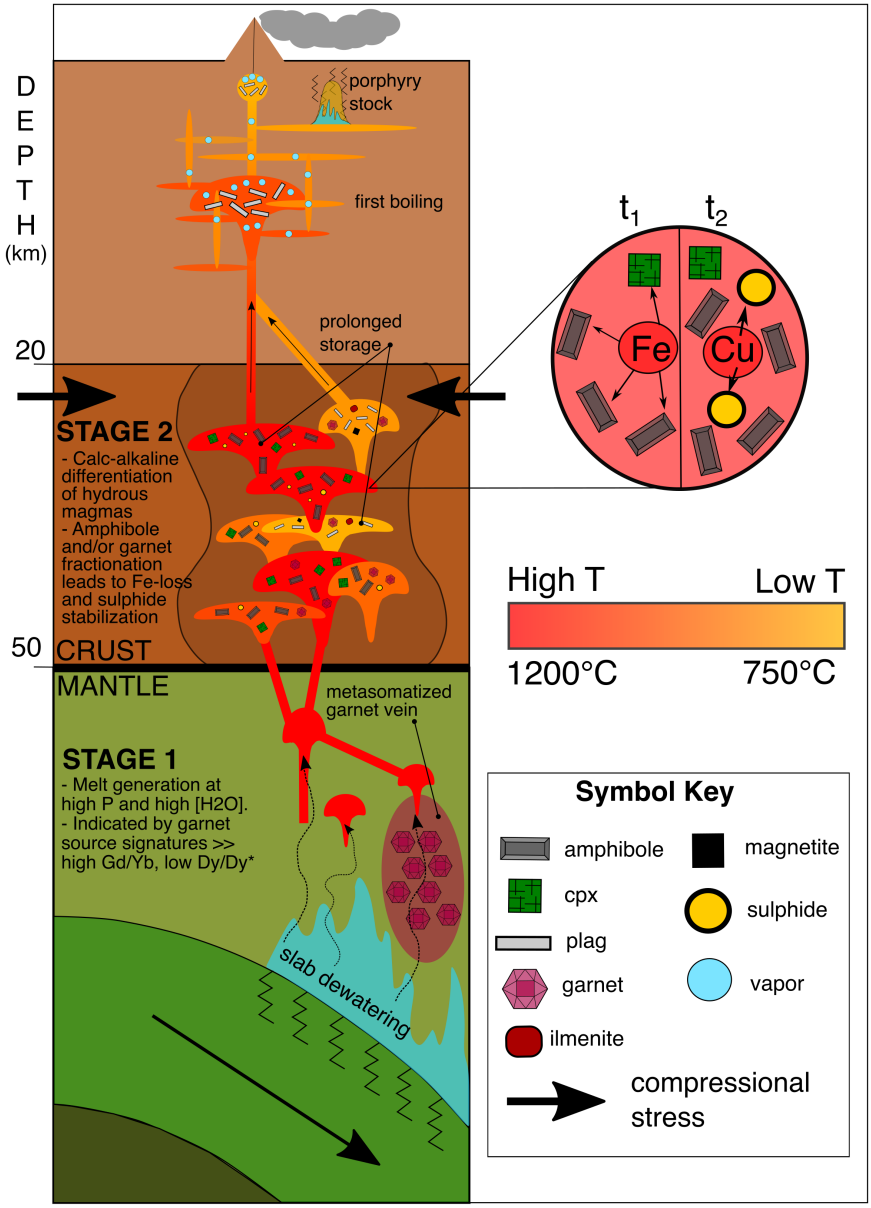

Figure 8: Our proposed model for Cu depletion in arc magmas. This model takes into account the different geochemical and geophysical signals picked out by our database. Stage 1 sees hydrous melting stabilize garnet in the mantle wedge under the right conditions, which imparts the Gd/Yb signal seen in some magmas in Figure 7. High water contents of these calc-alkaline primitive melts contribute to prolonged amphibole fractionation in Stage 2, where magmas staled at depth (=/< 1 GPa) will fractionate enough amphibole to reduce [Fe] and stabilize sulphide. garnet fractionation likely plays a role at depths > 50 km, and could similarly deplete ore-fertile magmas in Fe, leading to sulphide fractionation.